DOI:
10.1038/s41592-018-0072-5

Document Version
Peer reviewed version

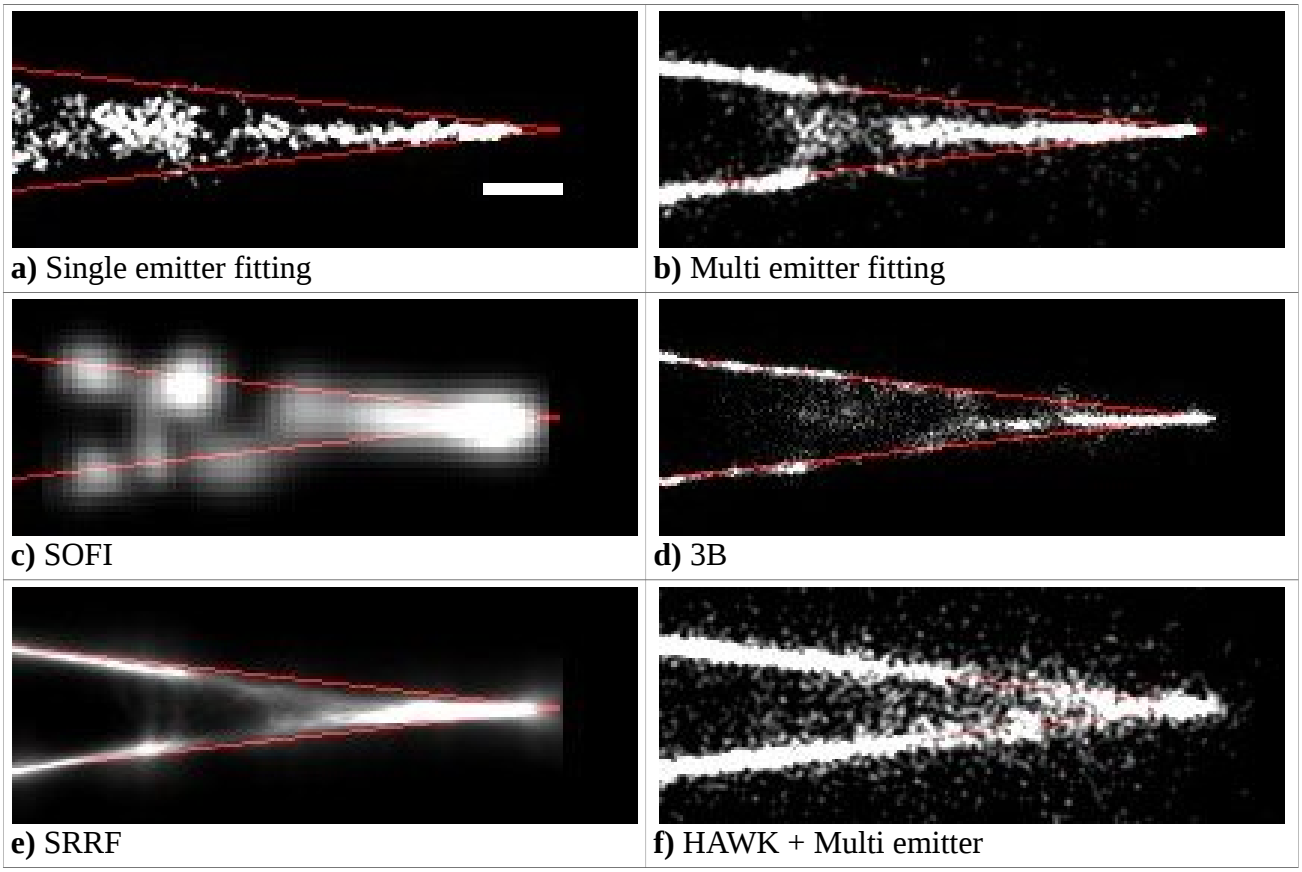

Supplementary Figure 1: Simulated Localization Microscopy data (256 frames) for converging lines of 10 nm width at an activation density of 2000 emitters / μm^2 of structure. Displayed is the region from 410nm to 10nm separation. The scale bar indicates the 270nm size of the PSF. Analysis performed using a) ThunderSTORM single emitter fitting, b) ThunderSTORM multi emitter fitting, c) SOFI 4th order, d) 3B, e) SRRF and f) HAWK analysis followed by ThunderSTORM multi emitter fitting. The red lines indicate the ground truth structure. At this extreme density, only by using HAWK can the structure be correctly resolved significantly below the diffraction limit. All other methods show substantial sharpening and distortion of the reconstructed image, under reporting the separation at small distances. In contrast the HAWK filtered results shows a reduction in precision (sharpness) but a substantial gain in accuracy compared to the other methods. Reproducibility was ensured by simulating sufficient frames to significantly oversample the structure. Individual emitters made an expected average of 8.53 separate appearances for a mean total of 42.7 frames each.

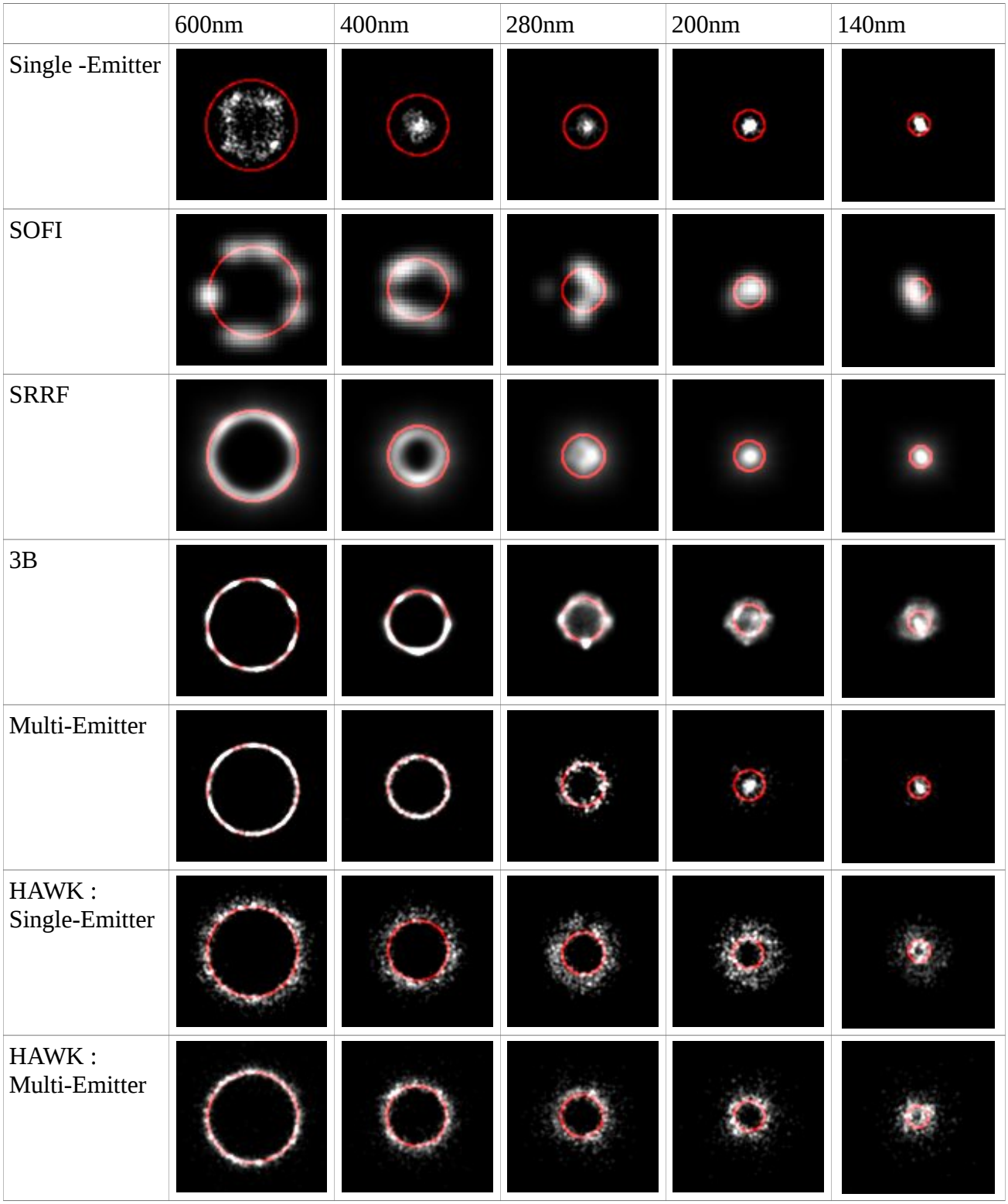

Supplementary Figure 2: Simulated LM data (256 frames) of circular structures at 1000 emitters / μm^2. The diameter of the circles ranged from 600 to 140nm, as indicated. Data was analysed using single emitter ThunderSTORM, SOFI, SRRF, 3B, multi emitter ThunderSTORM, HAWK analysis with single emitter ThunderSTORM and HAWK analysis with multi emitter ThunderSTORM. Red lines indicate ground truth. The two ThunderSTORM results and SRRF not only fail to resolve the hole in the smaller structures, but also under-report the size. SOFI and 3B results reflect the size of the structure but not necessarily its circular shape. HAWK analysis combined with ThunderSTORM gives results which reflect the circular nature of all the structures. Reproducibility was ensured by simulating sufficient frames to significantly oversample the structure. Individual emitters made an expected average of 4.66 separate appearances for a mean total of 23.3 frames each.

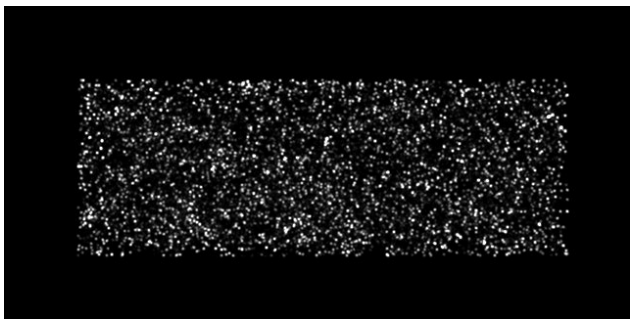

a) Low density: Single Emitter

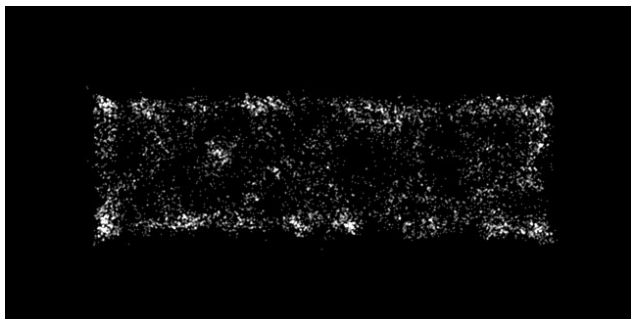

b) High density: Single Emitter

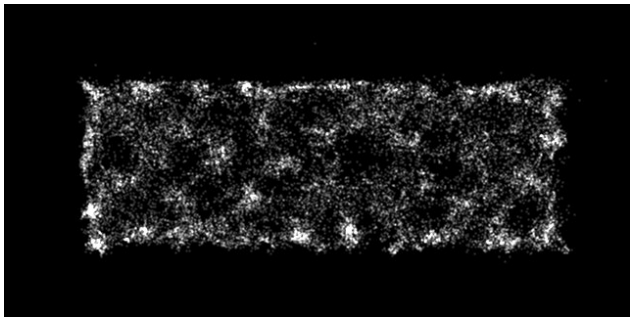

c) Multi Emitter

d) SOFI

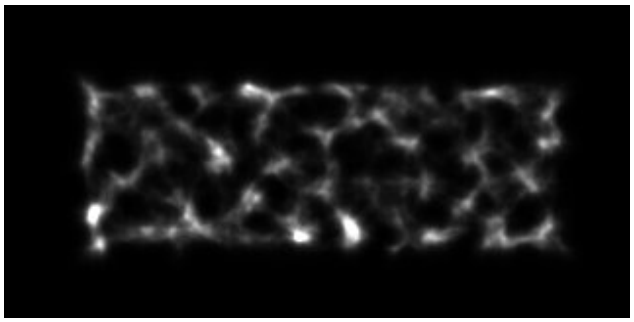

e) SRRF

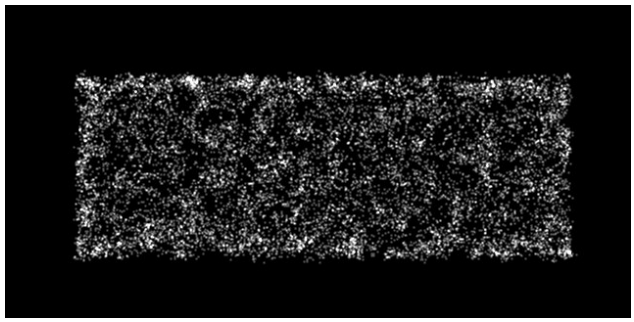

f) HAWK: Single Emitter

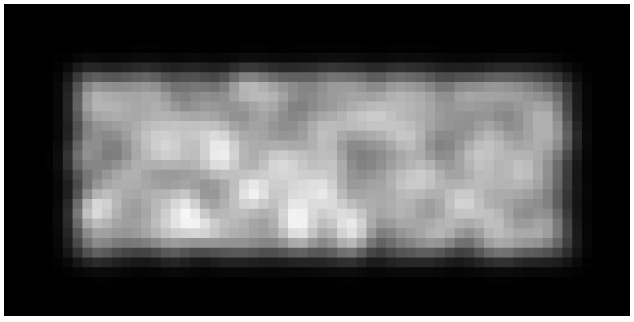

g) Ground truth : PSF

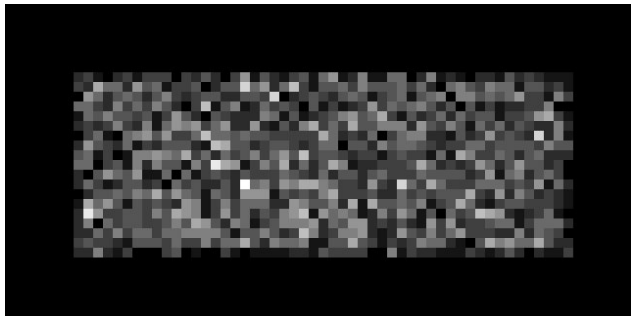

h) Ground Truth : bin x10

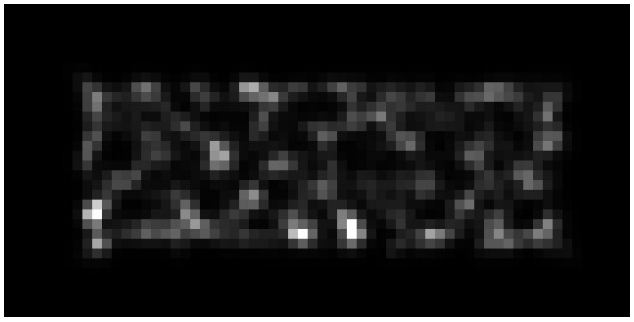

i) SRRF : bin x10

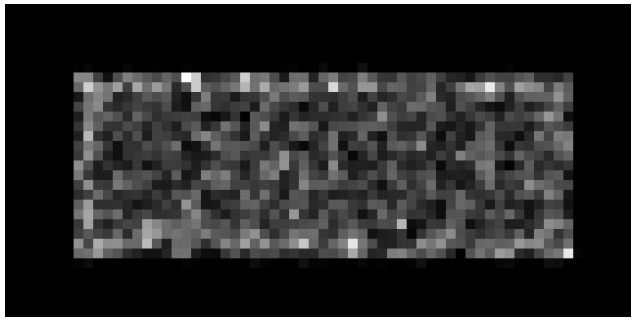

j) HAWK : bin x10

Supplementary Figure 3: Simulated results for randomly labelled 2-dimensional structures (5 μm x 1.8 μm) showing the artificial clustering patterns of many high density algorithms, which can also be eliminated with HAWK. The labelling density was 400 / μm^2 and the emitter density in each frame either 36 / μm^2 (high density) or 0.4 / μm^2 (low density). As the fluorescent emitters are

randomly distributed within the rectangle perfect reconstructions should show no structure at any scale (confirmed by Fourier analysis of the ground truth). Single emitter fitting of the low density data (a) correctly reproduces this lack of internal structure. However when applied to the high density data not only is the size of the structure significantly under estimated, but it also contains significant clustering of the localisations within it.

The high density methods multi-emitter fitting, SOFI and SRRF (c-e respectively) better reproduce the size but display much more pronounced internal structure. With HAWK and single emitter fitting (f) this tendency for artificial clustering in the reconstruction is almost completely eliminated. The origin of this clustering tendency can be demonstrated by examining the structural variation over larger length scales, e.g. 1 camera pixel (100nm). Panel (g) shows the ground truth for the above simulations convoluted with the PSF and averaged over the camera pixel size of 100nm (effectively the wide-field image). This appears to show substantial clustering of the random distribution of fluorescent labels which is not apparent if the original 10nm grid ground truth is simply averaged over the larger 100nm pixels (h). When the same 10x spacial averaging is applied to the super-resolution reconstructions substantial differences between the methods are observed. The SRRF reconstruction (i) show a very strong correlation with the wide-field image (g) and little resemblance to the ground truth (h). Multi emitter fitting (not shown) shows a similar, if not quite as pronounced, correlation with the wide-field. SOFI (also not shown) however, although showing structure/clustering not present in the ground truth image(h), these do not correlate with the wide-field image (g). The HAWK processed data (j) shows very little internal structure with almost no correlation with the wide-field but does resemble the ground truth (h) almost as well as the low density result (not shown). As HAWK and SOFI have been shown in the previous results not to induce significant artificial sharpening, unlike SRRF and multi-emitter fitting, this correlation with the wide-field image could perhaps be used as signature of failure due to too higher emitter density in these methods.

Reproducibility was ensured by simulating sufficient frames to significantly oversample the structure. Individual emitters made an expected average of 4.66 separate appearances for a mean total of 23.3 frames each.

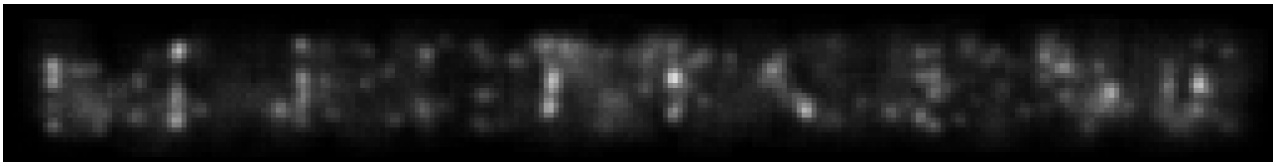

a) Example frame with out of focus background emitters.

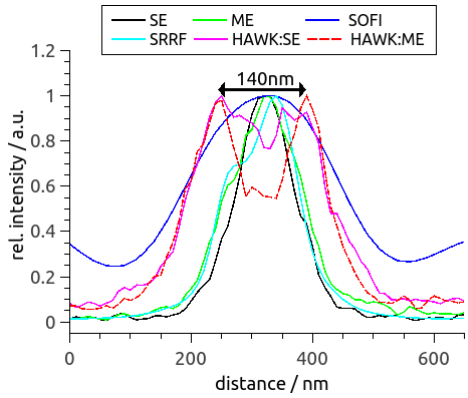

b) 140nm separation line profiles

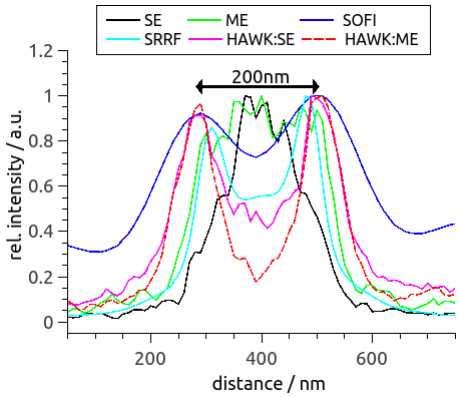

c) 200nm separation line profiles

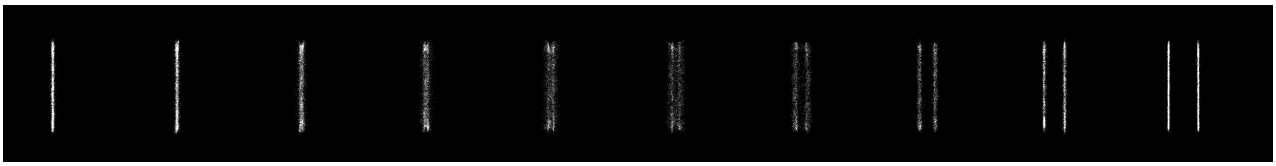

d) HAWK reconstruction of 'lines' simulation for low drift

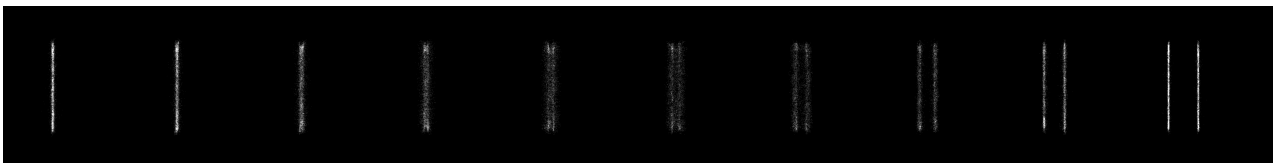

e) HAWK reconstruction for 'lines' simulation for very high drift

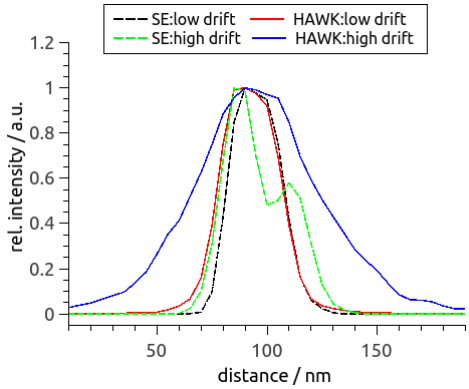

f) Single line widths from d) and e) above

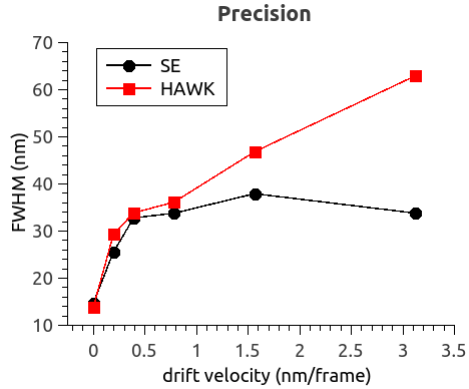

g) Variation in precision with drift velocity

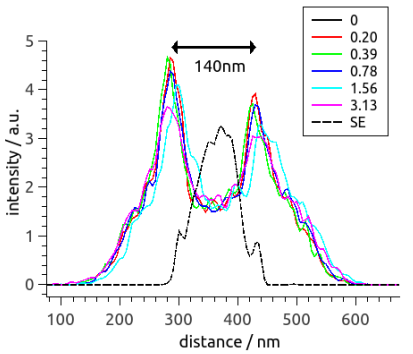

h) 140nm line profiles

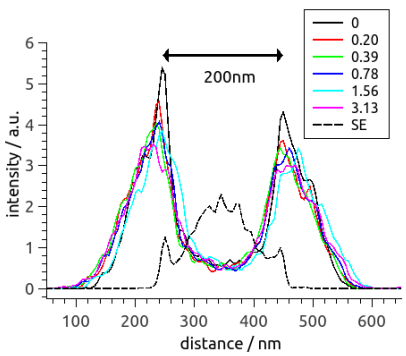

i) 200nm line profiles

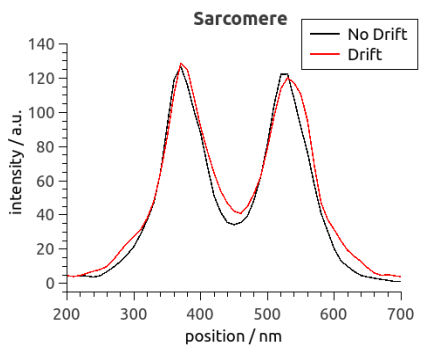

j) Sarcomere line profiles

Supplementary Figure 4 : Comparison of how the performance of HAWK is reduced by out of

focus background emitters and sample drift to other high density methods. Simulated structure is as the 'lines' simulation but with addition of an out of focus background (a-c) or sample drift (d-j). The out of focus background was simulated by a random distribution of emitters over *x*,*y* and 1μm in *z*. The line structures are position on the focal plane (*z*=0). The background emitters had their PSF enlarged according to their *z* heights to simulate an out of focus background. The blinking properties were the same as the 333 emitters per μm^2 simulation. The density of emitters in the background was 10% of that of the structure but the 2 dimensional nature means there are actually nearly 17 background molecules emitting for every structural label. An example frame from this simulation is shown in a).

Line profiles for the 140nm & 200nm separations are shown in b) & c) respectively for single emitter fitting and the high density methods. Comparison with the case for no out of focus background (see the main text) show reduced performance for all the high density methods. This is partly due to the defocused PSFs and partly the increased total emitter density. HAWK, whether it be with single or multi emitter fitting, still substantially out performs all the other high density methods.

Evaluation of the effects of sample drift for single emitter fitting with and without prior HAWK processing are shown in (d-j). Linear drift in the X direction (perpendicular to the lines) was applied to the 333 emitters / μm^2 'lines' simulation. Drift velocities of 0.20,0.39.0.78,1.56 and 3.13 nm / frame were applied to the 768 frame sequence, corresponding to 20,39,78,156,313 nm/s at 100Hz camera frame rate. The highest drift velocity corresponds to movement of 0.25 camera pixels over 8 frames which is the longest time-scale filter used (level 3) in the HAWK processing. Drift correction was applied using the cross correlation method. Example reconstruction using HAWK and single emitter fitting are shown in d) for 0.20 nm / frame and e) for 3.13 nm / frame show no obvious differences. The localisation precision was estimated from the width of one of the lines separated by 600nm as this distance is to large to be artificially sharpened. Example profiles for the lowest and highest drift velocities are shown in f) both with and without prior HAWK processing. The width of a Gaussian fit to the profiles at each drift velocity (along with no drift) is shown in g). Below 1 nm per frame the loss in precision is almost entirely due to the accuracy of the drift correction technique, with HAWK performing no worse then standard single emitter fitting.

Line profiles from the 'lines' simulations for HAWK with single emitter fitting are shown in h) and i) for each drift velocity at 140nm and 200nm separations. These show the resolving power of HAWK is only very slightly reduced by even substantial drift. The unprocessed single emitter reconstructions with no drift are shown for comparison. A similar result is found for the T12-sarcomere data (j) that shows very little difference with 0.5nm/frame of simulated drift from the case with no drift added.

For simulations reproducibility was ensured by simulating sufficient frames to significantly oversample the structure. Individual emitters made an expected average of 4.95 separate appearances for a mean total of 24.8 frames each. Simulated drift was not tested on other experimental data.

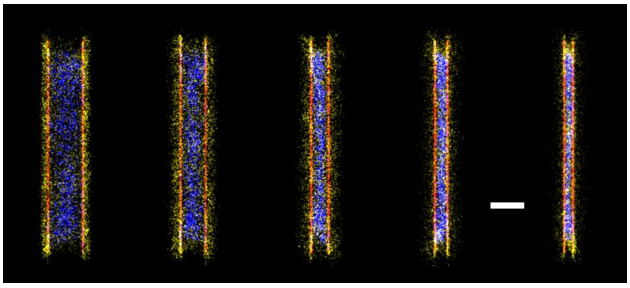

a) HAWK + Single emitter ThunderSTORM

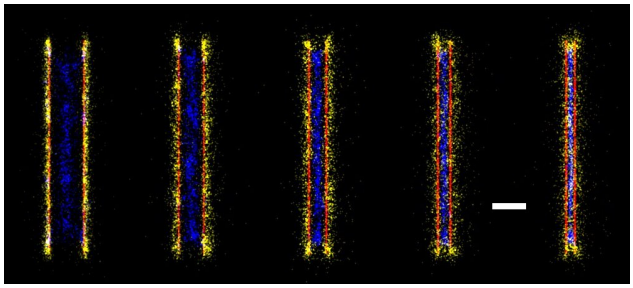

b) HAWK + Multi emitter ThunderSTORM

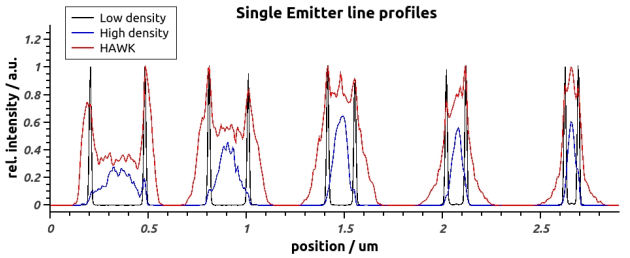

c) Line profiles from (a)

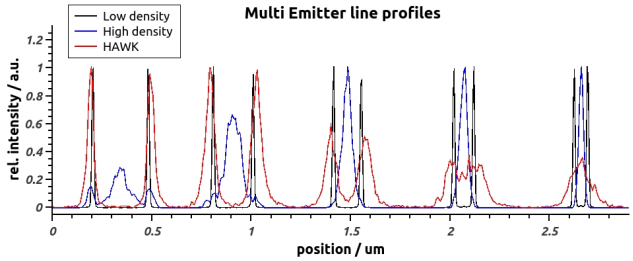

d) Line profiles from (b)

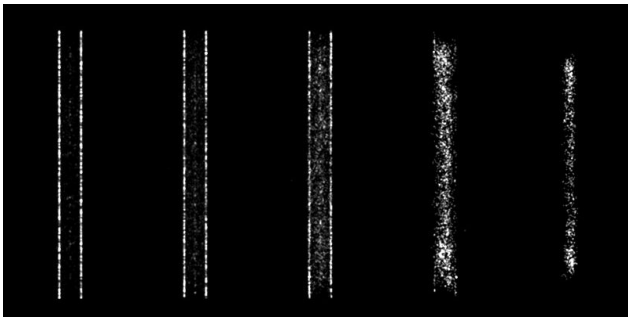

e) 140nm Single Emitter

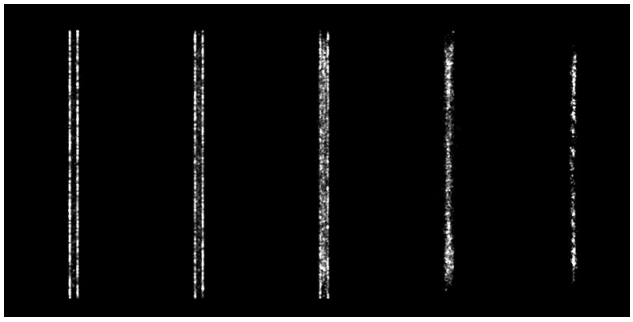

f) 50nm Single Emitter

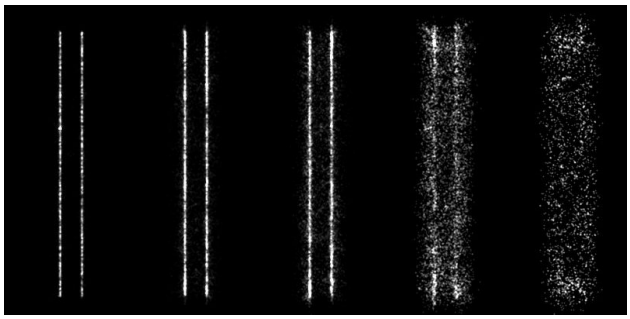

g) 140nm HAWK:Single Emitter

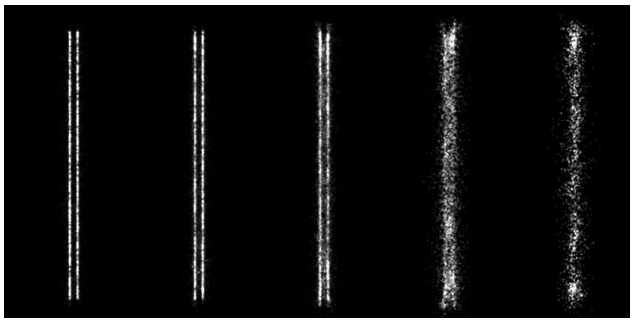

h) 50nm HAWK:Single Emitter

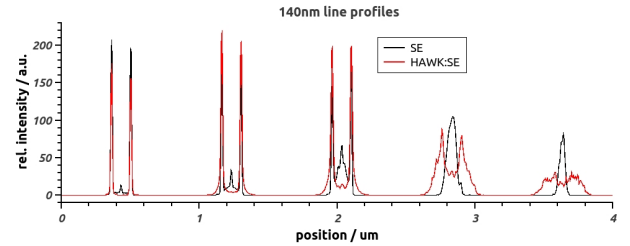

i) Line profiles from (e) and (g)

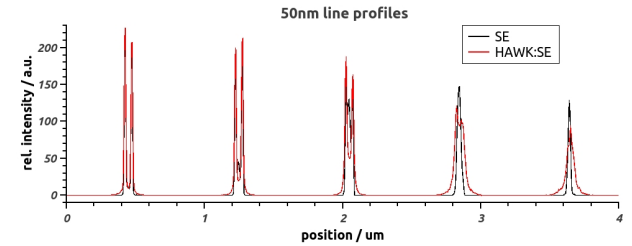

(j) Line profiles from (f) and (h)

Supplementary Figure 5: Simulated LM data for pairs of parallel lines of different spacings and different emitter densities. Top panels (a&b) show reconstructions for various line separations. (Left to right : 280nm, 200nm, 140nm, 100nm and 70nm) with and without HAWK analysis. a) Comparison for single emitter ThunderSTORM fitting without HAWK analysis (blue) and with HAWK analysis (yellow) with the single emitter low density reconstruction (red). High density data had 768 frames at 333 emitters / $\mu m^{2,}$, whilst low density had 25,600 frames at 10 emitters / μm^2 . The scale bar is 270nm (which was the PSF FWHM). b) As a) but using multi emitter ThunderSTORM and using 256 frames at 1000 emitters / μm^2 for the high density data. c & d) Line

profiles of a&b respectively. The same scaling factor has been applied to all data, so the difference in integrated area reflects the relative number of localisations.

With both single and multi emitter fitting the unprocessed data show substantial sharpening in the reconstructions. Not only are all the line pairs unresolvable but the resulting structure is significantly narrower than the ground truth (as indicated by the low density results). With HAWK analysis many line pairs are resolvable, and where they are not the width of the resulting structure is comparable to that of the underlying structure.

(e-j) Variation of accuracy of super-resolution reconstructions with emitter density on simulated line structures. (e-h) Single emitter reconstructions of line pair simulations at (from left to right) 10, 33, 100, 333 and 1000 emitters / μm^2. e) 140nm spacing without HAWK analysis, f) 50nm spacing without HAWK, g) 140nm with HAWK and h) 50nm with HAWK. (i-j) show the line profiles of (e-h). Without HAWK (e&f) the reconstructions show filling in between the lines and artificial sharpening and shortening as the emitter density is increased.

With HAWK analysis the lines are better resolved at intermediate density and can be resolved up to a much higher density. Once lines are no longer resolvable the sharpening and shortening effects are not present and the end distortions are reduced.

Reproducibility was ensured by simulating sufficient frames to significantly oversample the structure. Individual emitters made an expected average of 4.66-5.11 separate appearances for a mean total of 23.3-25.6 frames each.

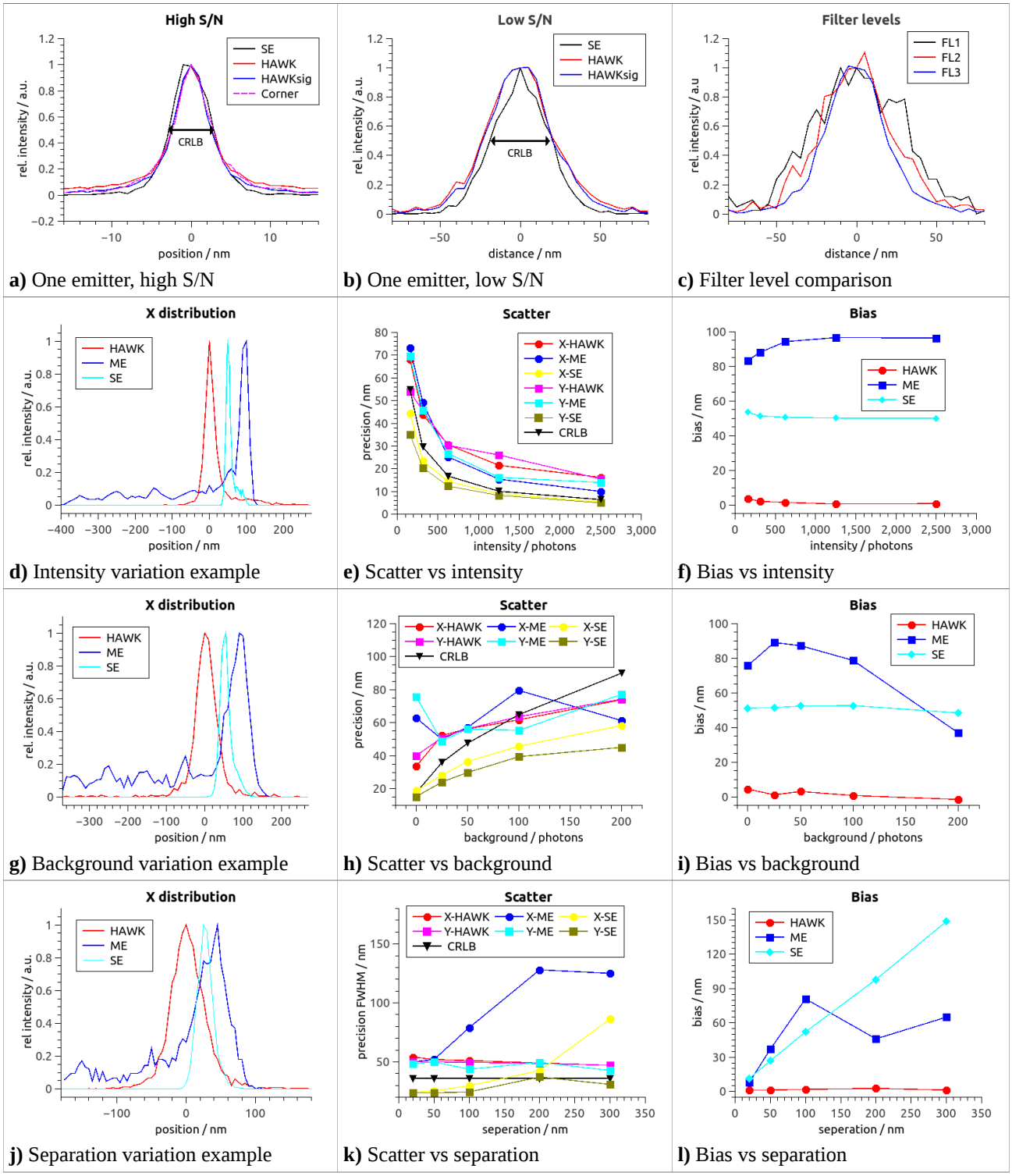

a) One emitter, high S/N **b)** One emitter, low S/N **c)** Filter level comparison

d) Intensity variation example **e)** Scatter vs intensity **f)** Bias vs intensity

g) Background variation example **h)** Scatter vs background **i)** Bias vs background

j) Separation variation example **k)** Scatter vs separation **l)** Bias vs separation

Supplementary Figure 6 : Evaluation of the localisation precision and accuracy with HAWK against variations in the emitter brightness background level and inter-emitter separation. Results are for repeat localisations of a simulated single emitter either in isolation (a-c) or in close proximity to another (d-l). The distributions of the x localisation coordinate are shown in a) for the case of a mean emitter density of 2500 photons and zero background light. Maximum likelihood Gaussian fitting with and without HAWK both show a FWHM close to the estimated Cramer-Rao lower bound (CRLB = 5.6nm). The HAWK data show a slightly longer tail and a small baseline to the distribution compared to the unprocessed data. This is due to false positive localisations brought about by (shot) noise as described in the text. The HAWKsig data have most of these false localisations and therefore the tail of the distribution removed by filtering out localisations with non-physical PSFs (sigmas >60 & < 130). Also shown are the HAWKsig results with the emitter located at the corner of a camera pixel rather than the centre, indicating the are no relative pixel

location effects with HAWK. For an emitter intensity of 250 photons and a background light level of 25 photons per pixel (b) HAWK only results in a very slight reduction of precision over unprocessed data (CRLB = 35.9 nm, SE = 40.4nm, HAWKsig = 42.8nm). Distributions for each individual filter level used in (b) are shown in (c). Longer times scale Haar filters show an increase in precision (level1 = 69.0nm, level2 = 50.7 nm, level3 = 41.2nm). This is to be expected as the longer time-scale filters combine information from multiple frames, and average out noise.

The second row (d-f) shows how the localisation precision (as measured by fitting a Gaussian to the scatter of localisations) and accuracy (bias) are effected by emitter brightness (156, 313, 625, 1250 & 2500 photons / frame) for a constant background (25 photons / pixel). HAWK processing with single emitter fitting is compared to unprocessed multi and single emitter fitting for two simulated emitters at 100nm spacing. The multi emitter results only include frames where two emitters were identified by the algorithm so excludes those instances where the emitter pair produce a single localisation at there centre. Unprocessed single emitter results only include frames where both emitters where known to be 'on' in the original simulation. The distributions in the x coordinate are displayed in d) for an emitter intensity of 625 photons per frame (background 25 photons/pixel for all intensities). For single emitter fitting localisations are sharply distributed about the central position between the two emitters. A small tail to the distribution results from dimmer emitters that switched off mid frame. The multi emitter results show a sharp peak biased away from the true position (x=0) with a very broad and skewed tail. The peak is largely due to false positives but gives the appearance of high precision. The true positives have a much larger variance. The HAWK localisations are highly centred about the correct position. The slight tale to the positive x side is due to filter 'bleed through' from the emitter located at x=100nm, leading to a small number of false positives. The results of fitting Gaussian functions to these distributions is shown in e) for the FWHM (scatter) and f) for the offset from zero (bias). These show HAWK achieves compatible precision to multi emitter fitting but much lower bias than either single or multi emitter fitting. Although single emitter fitting appears to exceed the precision of HAWK and the CRLB, this is because these localisations only result from fitting a single Gaussian to two emitters (twice the photons). This is particularly significant when the signal to background is low.

A similar result is found for the variation of scatter/precision and intensity (250 photons in each case) with background light level (g-i). The example distribution in g) is for 25 photons per pixel. Again HAWK shows comparable precision but much lower bias. For very high background light levels the precision of all methods seam to be higher than the CRLB. For SE this is for the same reason as above. In the case of the ME results it is because the standard deviation of the distribution (what is what is actually limited by the CRLB) is much greater than the width of the peak fitted by a Gaussian. This is to a much lesser degree also true of the HAWK data, but as HAWK is including information from multiple frames rather than just one the CRLB does not apply in the same way.

The variation of scatter/precision and bias with emitter separation is shown in j)-l). The emitter brightness and background level were kept constant at 250 photons and 25 photons/pixel respectively. The example distributions in j) are for 50nm separation. Here because of the greatly changing shape of the ME distribution with distance (multiple peaks appearing at larger separations) the scatter and bias are calculated differently, using the mean position and standard deviation (converted to a FWHM) respectively. SE fitting and HAWK distributions remain Gaussian like and are analysed as before. Under this measure HAWK shows much better precision as well as bias, particularly where the separation is 1-2 camera pixels. Distributions where produced from simulations consisting of 25600 frames with an expected 2327 frames containing both emitters in the 'On' state.

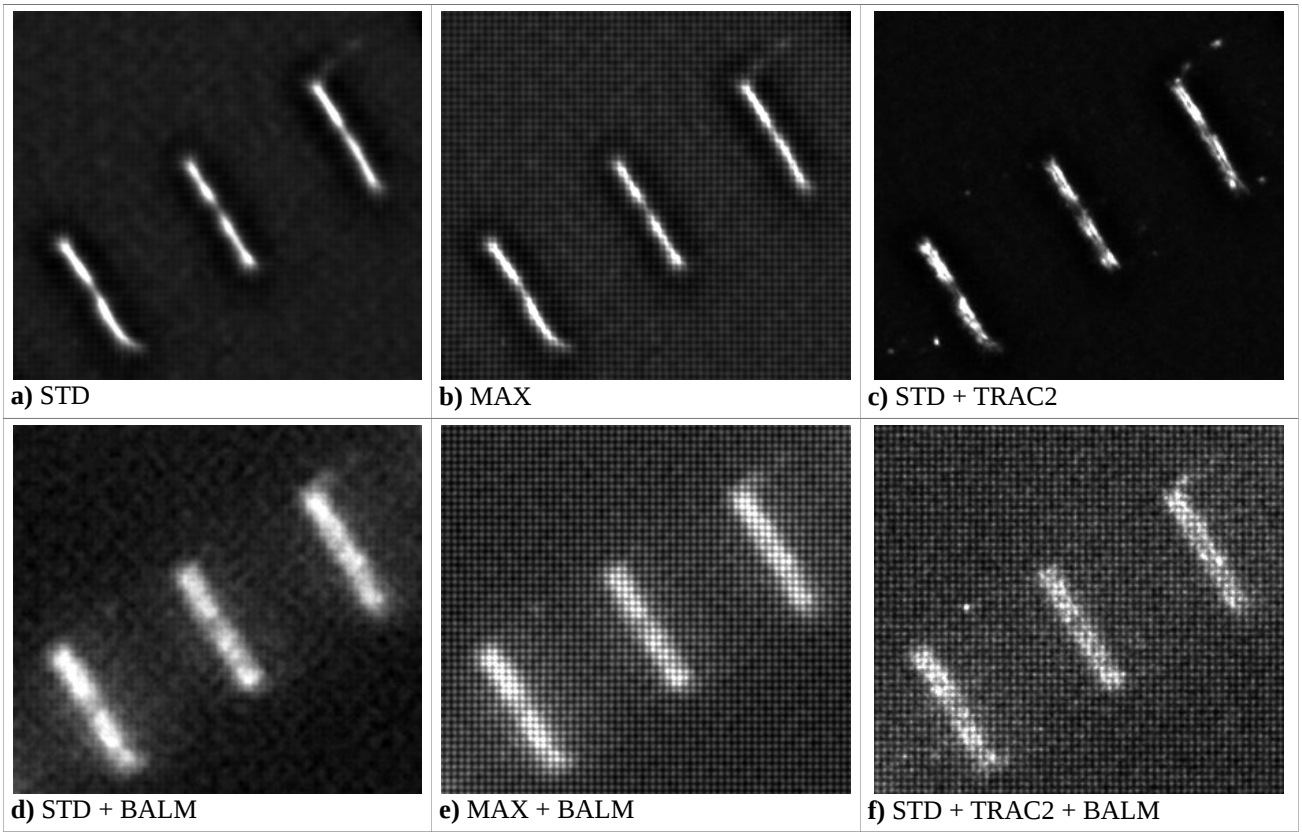

a) STD **b)** MAX **c)** STD + TRAC2

d) STD + BALM **e)** MAX + BALM **f)** STD + TRAC2 + BALM

Supplementary Figure 7: SRRF reconstructions of the muscle sarcomere data used in Figure 1 of the main text, using various combinations of settings. STD indicates standard (default settings). MAX indicates an increase in the magnification from x5 to x10, an increase in the axes in the ring from 6 to 8 and a decrease in the ring radius from 0.5 to 0.3. +TRAC2 indicates a change in the temporal analysis mode from 'Temporal pairwise radiality product mean TRPPM' to 'Temporal radiality auto-correlations TRAC' with TRAC order 2. + BALM indicates selection of the frame subtraction option. Frame subtraction (d-f) greatly reduces the amount of artificial sharpening in the image but substantially increases the amount of fixed pattern noise.

The temporal radiality auto-correlation option (c) appears to give partially resolved lines, but analysis of the profile indicate the separation is much too small, a result of artificial sharpening. This can be confirmed by the much broader image obtained by including the BALM option (f).

As a demonstration, only this experimental dataset was analysed using all settings combinations. These and other settings combinations where applied to simulated 'lines' and 'vee' data that showed similar trends.

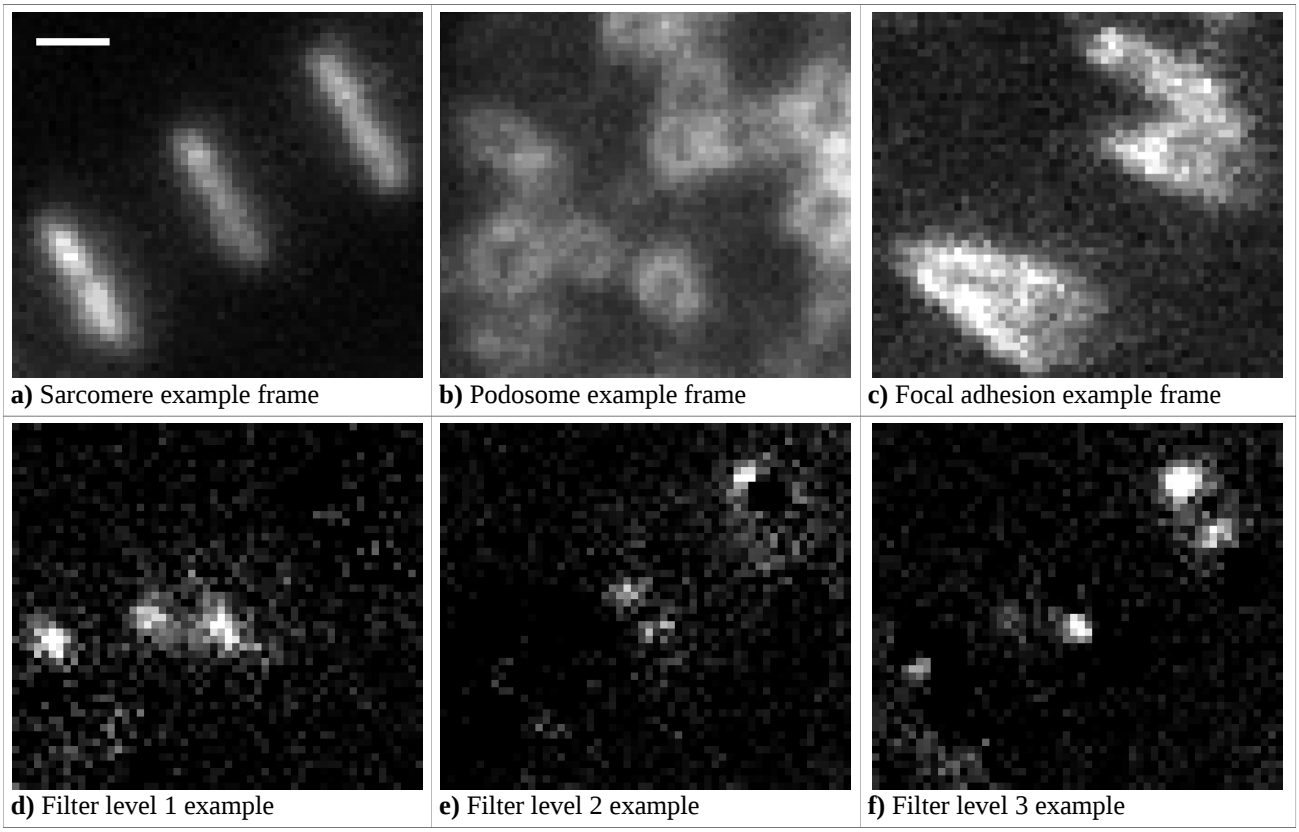

a) Sarcomere example frame | **b)** Podosome example frame | **c)** Focal adhesion example frame

d) Filter level 1 example | **e)** Filter level 2 example | **f)** Filter level 3 example

Supplementary Figure 8: Example raw data frames from the unprocessed and HAWK processed images sequences. The top row show sections of example frames from the unprocessed image sequences for the sarcomere (a), podosome (b) and focal adhesion (c) experimental data, indicating the very high emitter densities in these measurements. In each case the degree of emitter PSF overlap is sufficient that individual emitters cannot be resolved. The lower panels (d,e & f) show an example HAWK processed frame from each of the first 3 Haar filter levels described in the methods section for the sarcomere data at the point in the sequence displayed in a). The effective density is drastically reduced and the single emitter fitting algorithm has no difficulty resolving individual emitters. All images are at the same scale, scale bar 1 μm. Images are representative examples from at least 2389 frame long sequences.

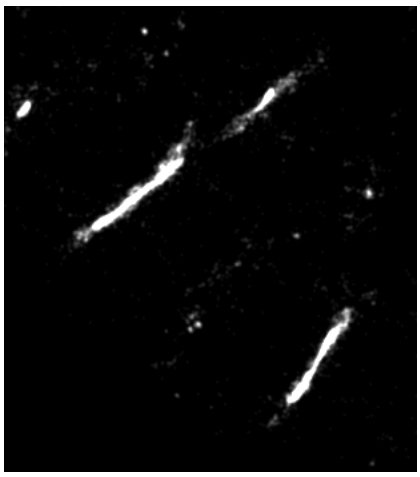

a) Single Emitter

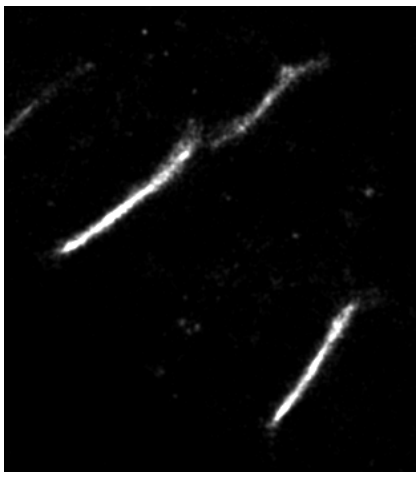

b) Multi Emitter

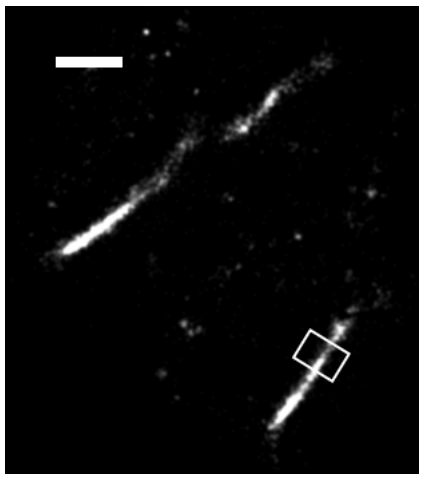

c) ME : sigma filtered

d) SOFI

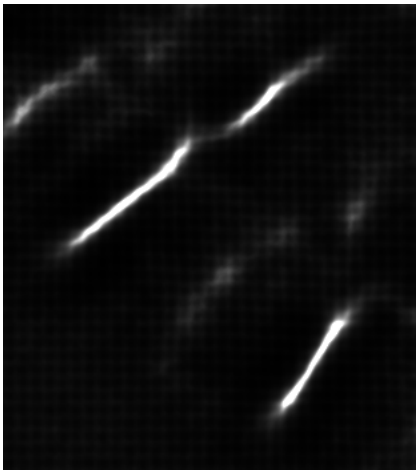

e) SRRF

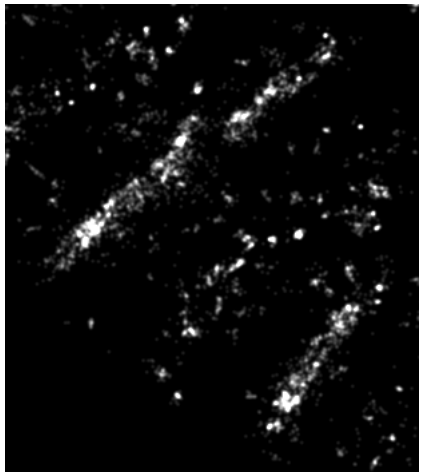

f) HAWK

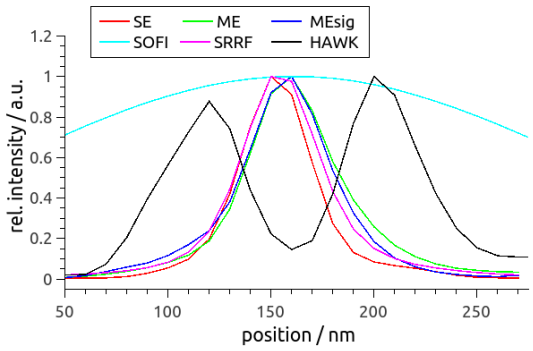

g) Line profiles

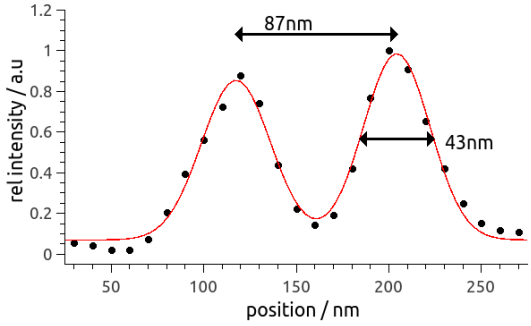

h) HAWK line profile fit

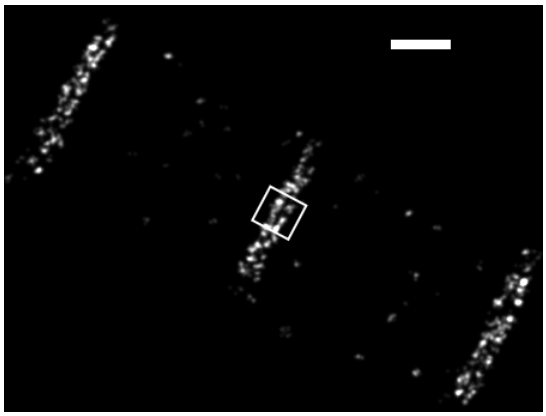

i) Low density cardiac M8 sarcomere

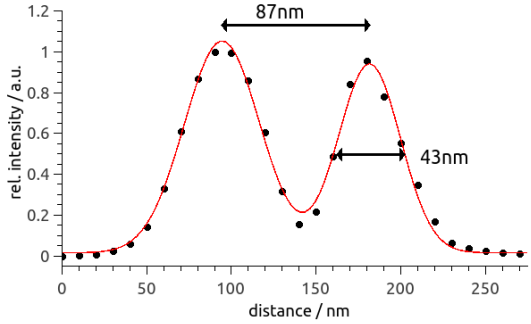

j) Low density line profile fit

Supplementary Figure 9 : Comparison of HAWK with other high density methods for M8-AF647

antibody labelled cardiac muscle sarcomeres. Comparison of HAWK-single emitter fitting (f) with unprocessed single emitter fitting (a) and other high density methods (b-e). Multi emitter fitting (b) even with additional filtering of poor (large sigma) localisations (c) performs no better than single emitter fitting. SOFI (d) shows a very broad single line but the ca. 90nm expected separation is beyond the theoretical limit when only used to the 4th order. SRRF (e) also shows extreme sharpening like the Gaussian fitting methods but also some fixed pattern noise. With prior HAWK processing the line spacings can be clearly resolved. Line profiles from the boxed region in c) are compared in g) and a fit to the HAWK profile is shown in h). A low density single emitter reconstruction is shown in i), and a fit to its line profile in j). Hawk shows comparable resolution to the low density case, the measured separation agreeing to within 1 nm. Scale bars are 500nm. Results are representative of 5 high density and 6 low density independent experiments.

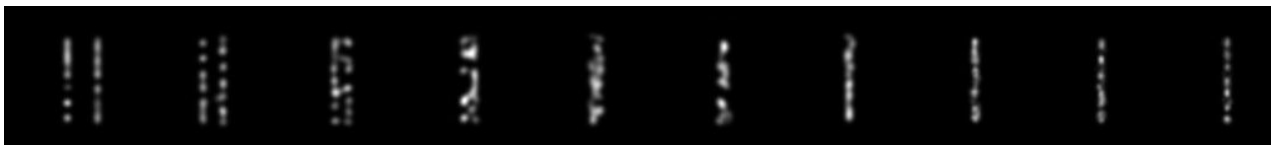

a) SOFI reconstruction of unprocessed simulated data.

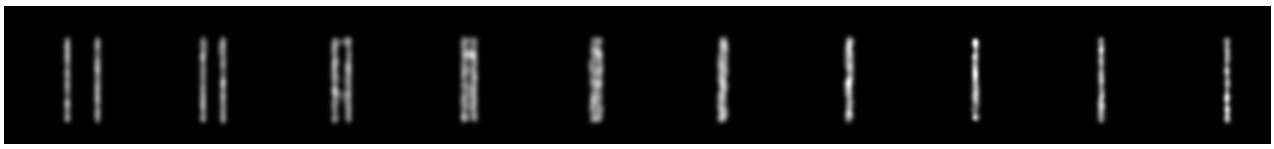

b) SOFI reconstruction of HAWK processed simulated data.

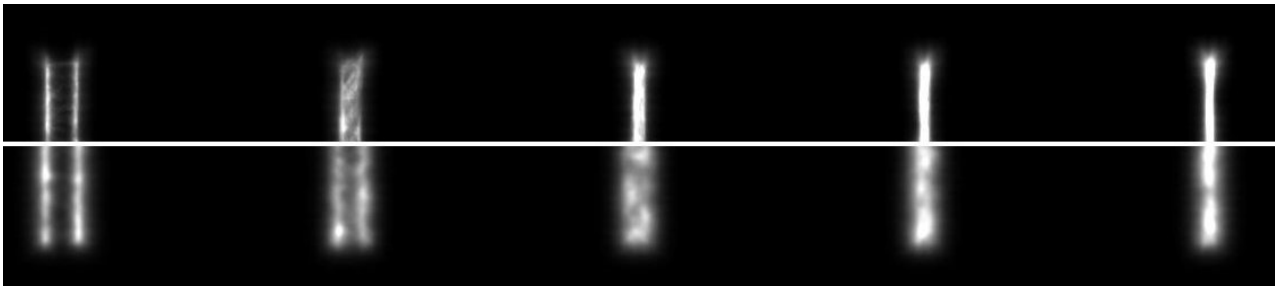

c) Comparison of SRRF with and without HAWK processing.

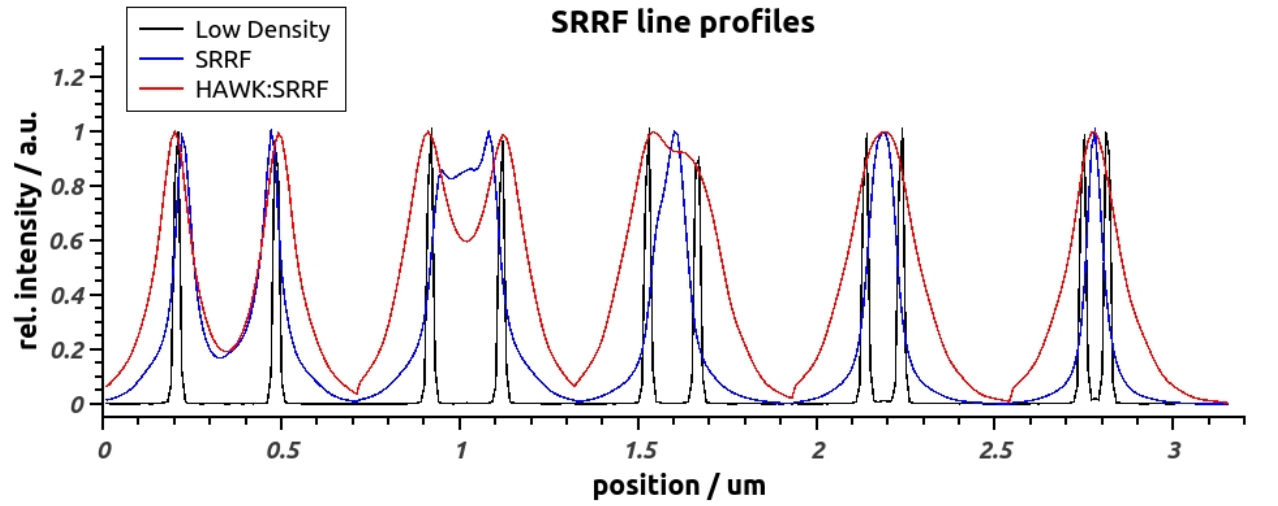

d) Line profiles from (c)

Supplementary Figure 10: Improved performance when using HAWK processing with other super-resolution algorithms on high density (1000 emitters / μm^2) simulated data. (a&b) Comparison of SOFI reconstructions of line structures with and without prior HAWK processing. Line spacings are 600, 400, 280, 200, 140, 100, 70, 50, 30 & 20nm. Unprocessed data (a) show substantial intensity variation. Lines separated by less than 280nm cannot be resolved. With HAWK analysis followed by SOFI (b) the lines appear more uniform and the resolution is slightly improved. c) Comparison of SRRF with HAWK analysis (bottom) and without (top) on line spacings of 280, 200, 140, 100 & 70nm. Line profiles of which are shown in d) along with those of the low density data. The accuracy of SRRF is clearly improved with HAWK. The SRRF profiles show substantial sharpening for the smaller separations (140, 100 & 70nm) compared to the low density ground truth. With HAWK although the lines cannot always be individually resolved, the reproduced structure is of comparable size to the underlying line spacing. As with the Gaussian fitting methods, when HAWK is used with SRRF the apparent resolution indicated by image sharpness is a good measure of the resolving power.

Reproducibility was ensured by simulating sufficient frames to significantly oversample the structure. Individual emitters made an expected average of 4.66 separate appearances for a mean total of 23.3 frames each.

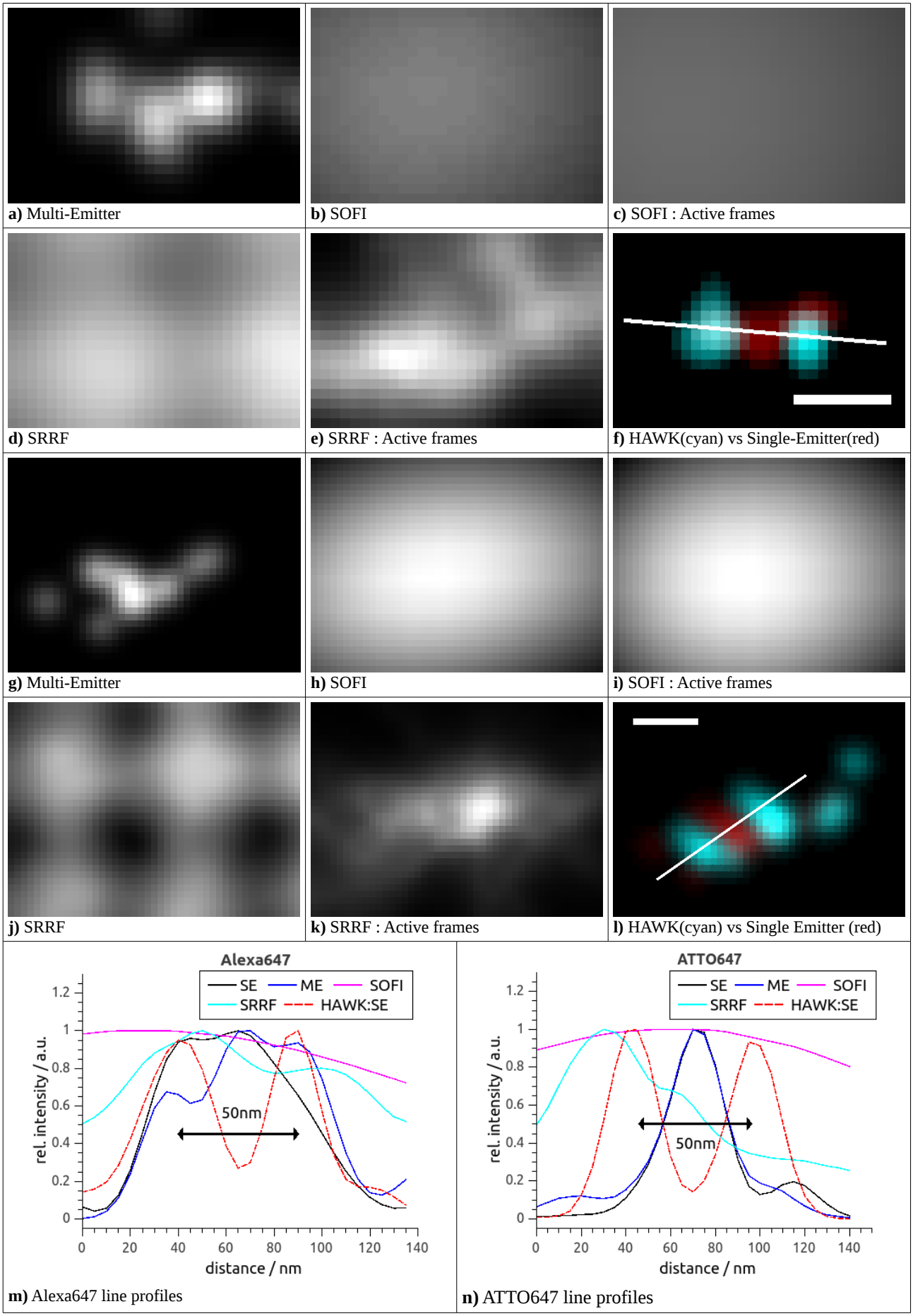

Supplementary Figure 11: Example reconstructions of 50nm DNA origami structures imaged at high density for the different high density methods. Top two rows are structures labelled with

Alexa647 (a-f), middle two rows (g-l) are for ATTO647 labelling. In both cases the SOFI results (b,c,h & i) for the entire image sequence produced a reconstruction totally dominated by a few very bright clustered objects leaving most of the structures undetected compared with single or multi emitter fitting. A 30x30 pixel subregion centred on the structured shown was therefore selected for analysis. Normal SRRF analysis (d,e,j & k) produced reconstructions dominated by fixed pattern noise. This likely arises because for any small sub region of the sequence the large majority of frames (5000 frame sequence) contain no active emitters. To reduce this tendency both the SRRF and SOFI results were reanalysed using much shorter frame sequences (25 frames for Alexa647, 30 frames for ATTO647, c,e,i & k) which the multi-emitter results indicated contained the majority of active emitters in this sub-region. HAWK processing (filter level 3) followed by single emitter fitting compared with unprocessed SE fitting using the entire image sequence is shown in f) & l). Scale bars are 50nm.

Results with Alexa647 and ATTO647 are very similar. SOFI shows no discernible structure as expected at this small scale. SRRF results show the presence of a DNA origami structure when the frames are restricted to active emitters but can't resolve the separation. Multi emitter fitting clearly indicates the presence of structures but it is difficult to unambiguously determine the number of structures of the flurophore separation. In both cases there appears to be a number of possible 'pair spots' that could be an origami structure but the apparent separation is too small or unclear. The HAWK reconstruction of the Alexa647 data (f) clearly display a single origami structure with two well resolved clusters of localisations at the correct separation (cyan). Overlaid is the single emitter result (red) that shows the substantial majority of localisations are positioned between the two ends of the structure (exactly the type of 'artificial sharpening' resulting from over-lapping flurophores predicted from the simulations). HAWK analysis of the ATTO647 data (l) again shows that without HAWK the single emitter localisations are predominantly positioned between the true flurophore positions due to fitting multiple overlapping emitters as a single one.

Measured line profiles for the above reconstructions are shown in m) & n). The SOFI and SRRF profiles are for the restricted (active) frame case. For the Alexa647 data ME fitting and SRRF produce a structure of the correct overall size but cannot resolve the separation of the two ends. Only with HAWK can this separation be clearly seen and is of the correct distance.

SRRF and SOFI analysis was only performed on these datasets.

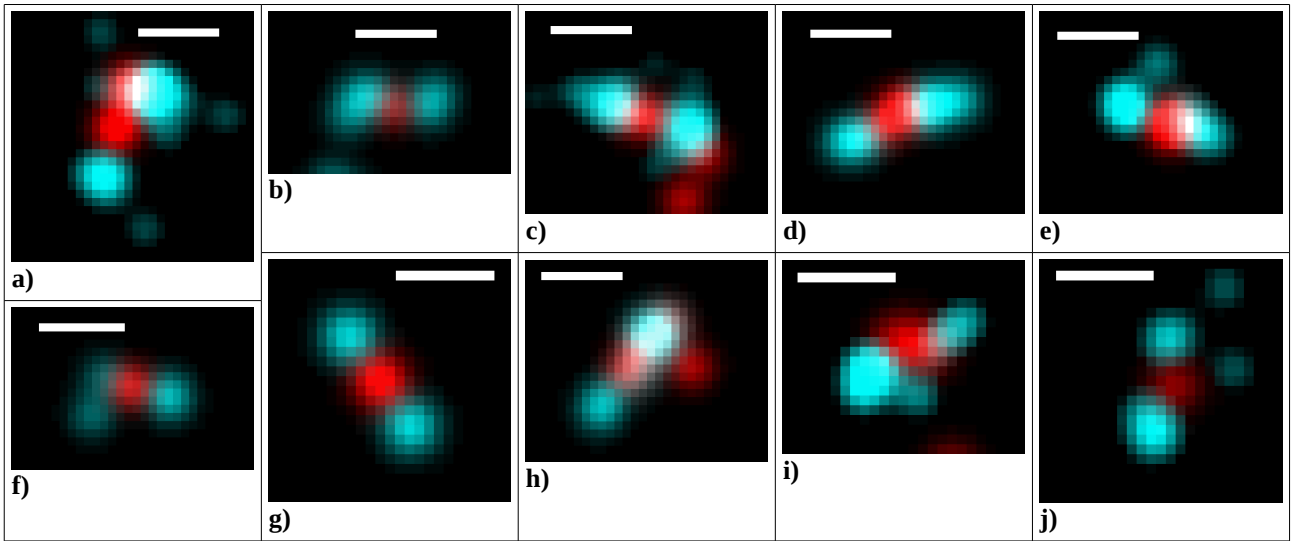

Supplementary Figure 12: Further example reconstructions of 50nm DNA origami structures. Comparison is between Single emitter fitting with (cyan) and without (red) prior HAWK processing on high density data. Top row (a-e) are for Alexa647 labelled structures and bottom row (f-j) are for ATTO647 labelling. In all cases the Hawk reconstructions show two clusters of localisation separated by 50±5 nm (measured from line profiles). Without HAWK the majority of localisations are positioned centrally to the two ends of the structures resulting from fitting to overlapping emitters at each end. Structures were selected from the reconstructions that clearly showed the effects of overlapping emitters and multiple localisations. Scale bars are 50nm. Representative examples where taken from 5 independent experiments (3 Alexa647, 2 Atto647).

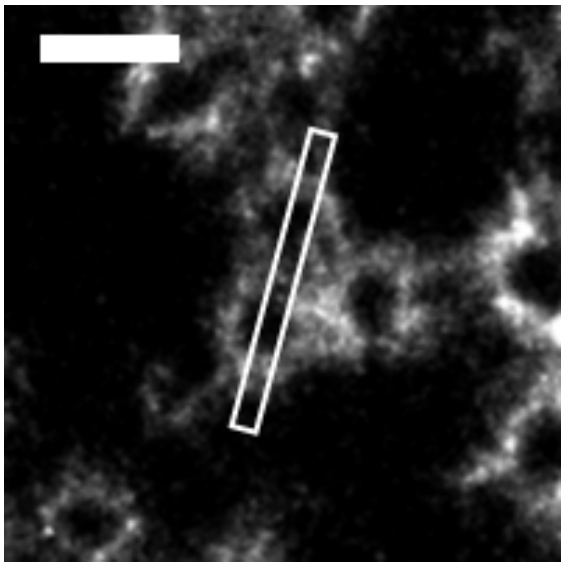

a) Podosome profile location

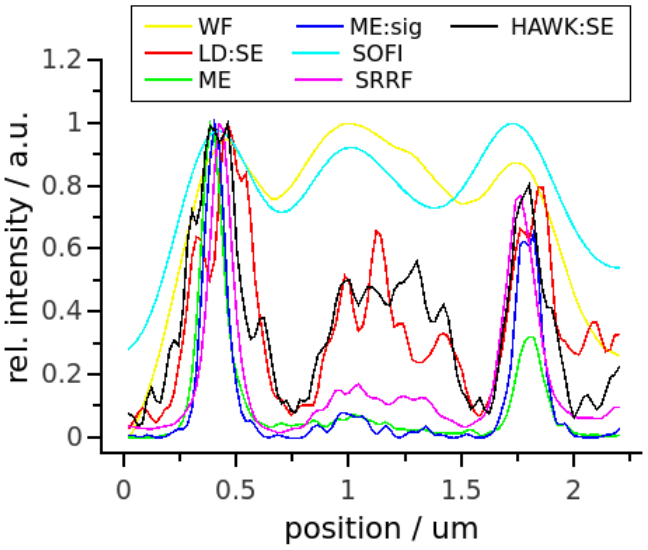

b) Podosome line profiles

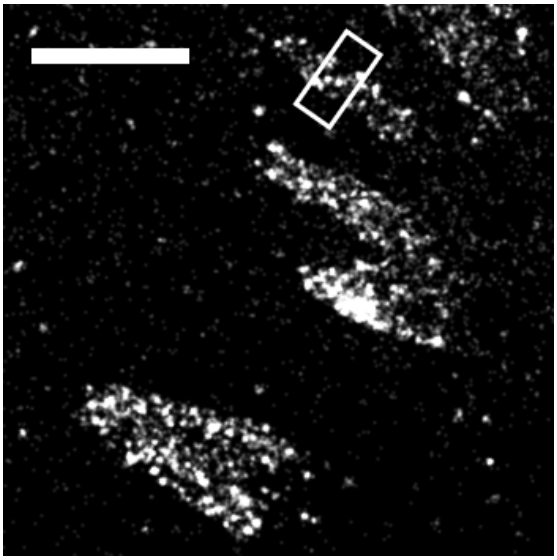

c) Focal adhesion profile location

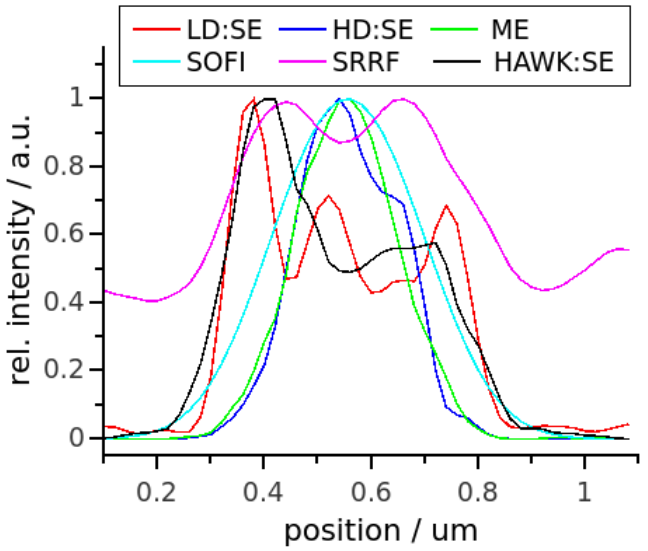

d) Focal adhesion line profiles

Supplementary Figure 13: Comparative line profiles for the different algorithms on the live cell data. Podosome data are displayed on the top row (a & b, scale bar 1 μm) and focal adhesion data on the bottom row (c & d, scale bar 2 μm). In each case the region over which the profiles are measured is displayed by the box on the low density reconstruction, with profiles averaged over the shorter dimension. For the podosome case the point where the two podosomes meet is clearly resolved in the low density data which is reflected in the line profile in b). This is also present in both the wide-field (taken by averaging all the high density frames) and SOFI profiles but is not as clearly resolved. Both the multi emitter and SRRF methods produce much narrower podosome ring widths compared to the low density reconstruction and some structure is missing. However, HAWK with single emitter fitting (black) shows excellent agreement with the low density profile (red) for both the presence of the central boundary and their thickness.

The width of a focal adhesion is displayed in d) for all the methods used in the main text. The low density profile was taken from a smoothed reconstruction (adjacent point averaging – ImageJ) as the density of localisations in the image was low. Again only the HAWK processed data (black) correctly reproduces the line profile from the low density reconstruction (red). SRRF gives a similar width but does not reproduce the steep sides, plateau or left hand peak of the low density profile as well as showing a substantial background. SOFI and particularly multi emitter fitting produced greatly sharpened images even of those structures that are approaching twice the width of the PSF. All high density live cell data showed better correlation of structural feature sizes to the

low density reconstructions with prior HAWK processing.

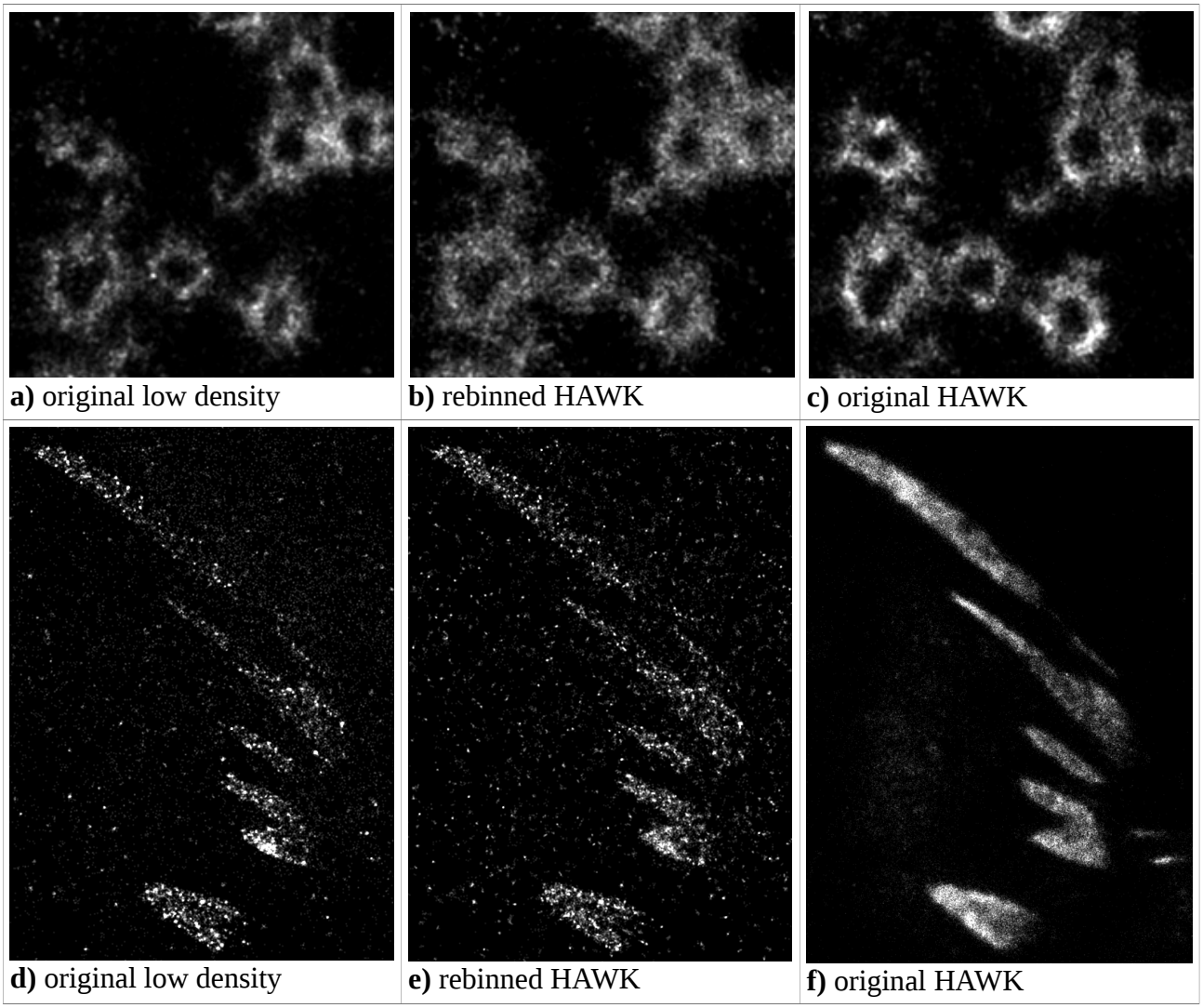

a) original low density | **b)** rebinned HAWK | **c)** original HAWK

d) original low density | **e)** rebinned HAWK | **f)** original HAWK

Supplementary Figure 14: Reconstructions on artificial intermediate density data sets made by summing 10 frames of the original low density podosome dataset (b) and 20 frames of the low density focal adhesion dataset (e). The number of frames summed was chosen to boost the emitter density as high as possible without reducing the signal to noise so much that the localisation precision fell to unacceptably low values. The variations in intensity of the rebinned HAWK reconstructions show much greater similarity to the low density reconstructions (a & d for podosomes and focal adhesions respectively), than the reconstructions on high density data (c & f respectively). This shows the intensity differences between high and low density reconstructions arises principally from the greatly differing number of localisations and some remodelling of sample structures over the time of the experiment, not a result of HAWK analysis. There is a noticeable reduction in localisation precision evident in the rebinned HAWK case (particularly the podosome data (b)). This results from the reduced brightness of the emitters relative to the background produced by summing frames and the 'averaging out' of some of the intensity fluctuations used by HAWK. As a demonstration of the methodology, only these image sequences was re-analysed in this way.

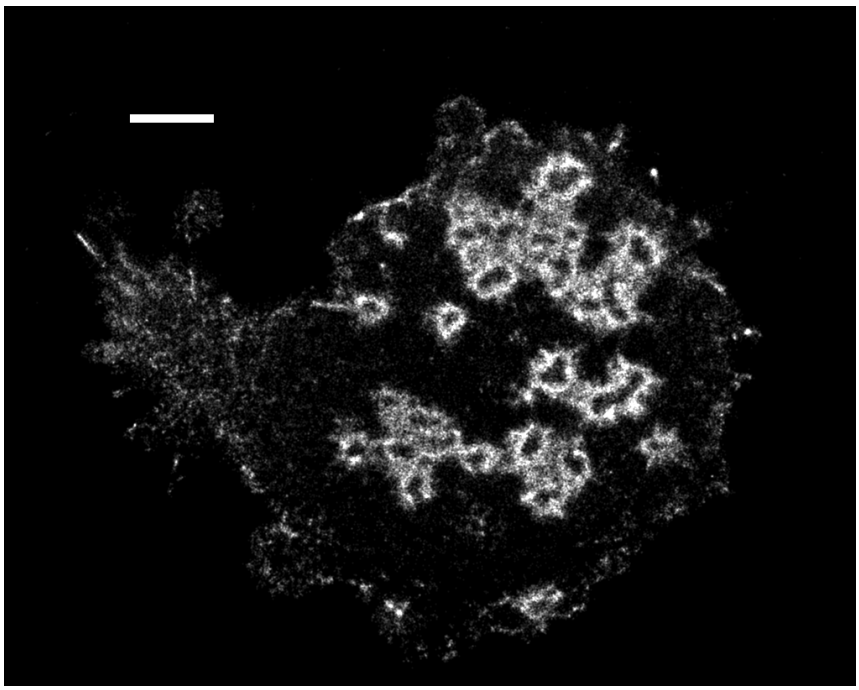

a) Whole cell, FRC = 110±1nm

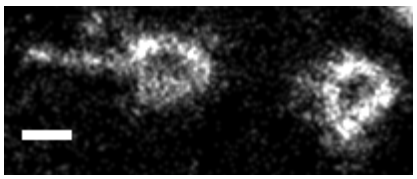

b) Podosomes FRC = 130±5nm

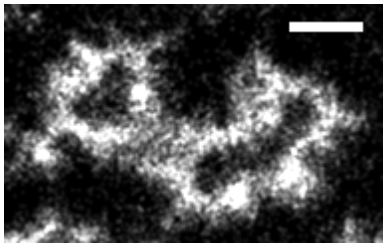

c) Podosomes FRC = 110±12nm

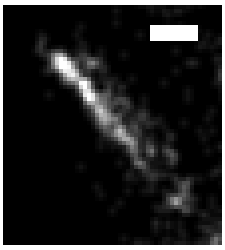

d) Focal complex FRC = 49±6nm

Supplementary Figure 15 : Variation of measured FRC resolution for different regions of the sample. The sample is mEOS3.2-vinculin expressed in podosomes as described in the main text. The HAWK reconstruction of the entire cell is shown in a). The image contains structures of varying 'sharpness' that will contribute to the overall FRC resolution. This includes the podosomes themselves, the cell boundary and the sharp 'focal complex' at the top left. The measured FRC resolution for the whole cell was 110±1 nm. The two podosomes located in the centre of a) treated in isolation (b) have a FRC resolution of 130±5 nm. The cluster to their right (c) however that show more inherent structure have an FRC resolution of 110±12nm. The 'focal complex' on its own (d) may represent a better measure of the obtained resolution, less dependent on the size of the underlying structure. FRC in this case gives a resolution of just 49±6 nm. The reconstruction had duplicate localisations removed (see methods). The scale bars are 2μm, 500nm, 750nm & 250nm for a-d respectively.

The potential acquisition speed of HAWK with live cells is demonstrated by examining just the first 400 frames (4 seconds) of the acquisition sequence. In this case the measured FRC resolution of the focal complex in d) was 63±8 nm. The cell displayed contained the greatest variation in scale of structural features of those imaged, therefore only this cell was analysed with FRC in this way. All FRC measurements were repeated 3 times each with the mean and standard deviation reported.

Filter Level Localisations						
	Level 1	**Level 2**	**Level 3**	**Level 4**	**Level 5**	
T12-Sarcomere	36%	26%	18%	12%	8%	Atto 647N
M8-Sarcomere	48%	32%	20%			AF 647
Podosomes	25%	25%	23%	17%	11%	mEOS-3.2
Focal adhesions	46%	31%	22%			mEOS-2

Supplementary Table 1 : Percentage of emitters visualised in each Haar filter level for the experimental data. The actual number of localisations is normally approximately equal or even rises for longer filters however this is due to individual emitters being images several times in the output frames. The number of localisations has therefore been divide by the length of the filter to produce the above data. The data indicate that AF647 'blinks' significantly more quickly than Atto647, as might be expected. The difference between mEOS-2 and mEOS-3.2 is perhaps more surprising and may be indicative of environmental factors.

Supplementary Note : Haar Wavelet Kernel Analysis Technique

HAWK analysis is an algorithm which is applied to the sequence of images acquired in a Localization Microscopy (LM) experiment. The output of this is an image sequence containing an increased number of frames with a lower number of emitters in each frame. The expanded image sequence is then analysed using an algorithm of the user's choosing.

The first step is to construct a set of pixel intensity traces from the unprocessed image sequence;

$$X(t)=\left\{I_{xy}(n=1),I_{xy}(n=2),\cdots I_{xy}(n=N-1),I_{xy}(n=N)\right\} \tag{1}$$

where x,y are the pixel indices and t is the frame number. For each pixel in turn its intensity trace X(t) (as a column vector) is multiplied by the Haar matrix to produce its transform trace Y(t').

$$Y(t')=H*X(t) \tag{2}$$

The non-zero elements of the Haar matrix are given by;

$$h_{i=1,j}=\left(\frac{1}{\sqrt{2}}\right)^{\log_2 N},\quad h_{i>1,j}=\frac{1}{2^{\lceil m/2\rceil}}*(-1)^k,\quad k=floor\left(\frac{j-1}{2^{\lceil m-1\rceil}}\right)$$
$$\frac{N}{2^m}+1\leqslant i\leqslant\frac{N}{2^{\lceil m-1\rceil}},\quad 2^m(i-1)+1\leqslant j+N\leqslant 2^m i,\quad m\leqslant\log_2 N \tag{3}$$

where i,j are the row and column indices, floor(..) indicates rounding down to the nearest integer and N is the total number of frames which must be truncated to an integer power of 2. The positive integer m represents the 'level' of the Haar Wavelet Transform (HWT). Each level corresponds to a differing length of fluorophore blinking in the original time trace, from the finest (m=1) to the coarsest (m=$\log_2$N) and a DC component, which for our purpose corresponds to intensity fluctuations (blinks) lasting from a single frame up to half the length of the image, plus a constant background (sample plus camera). The appropriate values of m will be discussed later. An example HWT for a simple 4 frame intensity trace is given bellow.

$$\begin{pmatrix}2\\0\\-\sqrt{2}\\0\end{pmatrix}=\begin{pmatrix}1/2 & 1/2 & 1/2 & 1/2\\1/2 & 1/2 & -1/2 & -1/2\\1/\sqrt{2} & -1/\sqrt{2} & 0 & 0\\0 & 0 & 1/\sqrt{2} & -1/\sqrt{2}\end{pmatrix}\begin{pmatrix}0\\2\\1\\1\end{pmatrix} \tag{4}$$

Here the different levels of the Haar matrix are coloured blue (m=1), red (m=2) and green (background).

The next stage is to apply the filter (level m) to the transformed intensity trace. This is done by setting all the elements of the column vector that don't correspond to that specific level of the Haar matrix to zero.

$$Y^{(m)}=\begin{pmatrix}\vdots\\0\\y_{a+1}\\\vdots\\y_{2a}\\0\\\vdots\end{pmatrix},\quad a=N/(2^m),\quad m\leqslant\log_2 N \tag{5}$$

To obtain the filtered pixel intensity trace the inverse HWT must be applied. The inverse of the Haar matrix is easily found as it is equal to its transpose.

$$H^{-1}=H^T \tag{6}$$

The filtered pixel intensity trace $Z^{(m)}$ is then given by:

$$Z^{(m)}(t)=H^T * Y^{(m)}(t') \tag{7}$$

Below is the inverse transform of the example above after filter level m=1 has been applied to the transformed intensity trace in equation (4) (colours as before).

$$\begin{pmatrix}-1\\1\\0\\0\end{pmatrix}=\begin{pmatrix}1/2 & 1/2 & 1/\sqrt{2} & 0\\1/2 & 1/2 & -1/\sqrt{2} & 0\\1/2 & -1/2 & 0 & 1/\sqrt{2}\\1/2 & -1/2 & 0 & -1/\sqrt{2}\end{pmatrix}\begin{pmatrix}0\\0\\-\sqrt{2}\\0\end{pmatrix} \tag{8}$$

Note that the filtered intensity trace contains odd-even frame pairs of equal magnitude but opposite sign. This is an inevitable consequence of using a single Haar frequency component, however the spatial correlation of the signs is physically meaningful. A cluster of positive values which is the same size of the PSF indicates an emitter increasing its brightness from an odd to an even frame. A similar cluster of negative values conversely indicates an emitter reducing in brightness. This provides a mechanism for separating On and Off transitions by cropping all negative values to zero in odd numbered frames, and cropping all positive values to zero and reversing the sign in even frames. This cropping procedure for the filtered intensity traces is described by the following equation:

$$\begin{Bmatrix}Z'^{(m)}(t)=Z^{(m)}(2t-1)\,\|\,Z^{(m)}(2t-1)>0, & Z'^{(m)}(t)=0\,\|\,Z^{(m)}(2t-1)\leq 0 & \ldots & t\leq N/2\\ Z'^{(m)}(t)=-Z^{(m)}(2t)\,\|\,Z^{(m)}(2t)<0, & Z'^{(m)}(t)=0\,\|\,Z^{(m)}(2t)\geq 0 & \ldots & t>N/2\end{Bmatrix} \tag{9}$$

where $Z'^{(m)}(t)$ is the cropped pixel intensity trace.

The transform-filter-inverse transform process is repeated for every pixel in the image sequence producing a set of filtered intensity traces $Z_{xy}^{(m)}$ from the set of unfiltered traces X_{xy}. These are then recombined to form a filtered image sequence $I_n^{(m)}$.

$$I_n^{(m)}=\sum_{xy} Z_{xy}^{'(m)}(t=n) \tag{10}$$

For the first level of filtering m=1 the HWT only compares intensity values with one of its two neighbouring frames. This can be easily rectified by repeating the process with all the wavelet

functions shifted by one frame (rotating the columns of the Haar matrix). Equally valid is to cyclically rotate the image sequence one frame. This will then compare even with odd frames (2 with 3, 4 with 5 …). The new pixel intensity traces are given by;

$$\left\{\begin{array}{l} X'(t) = X(t+1) \cdots t < N \\ X'(N) = X(1) \cdots t = N \end{array}\right\} \tag{11}$$

The process is then repeated on this new set of pixel intensity traces X'(t). The resulting image sequence is appended to the previous one resulting in twice the number of frames as the original data.

The final output image sequence is obtained by repeating the whole process for each of the desired filter levels m and appending the resulting image sequences together, producing a much longer image sequence than the original. When performing filter levels m >1 the output of equation 7 will produce $2^{(m-1)}$ duplicate frames. Before proceeding to equation 9 therefore all but every $2^{(m-1)}$ th element of $Z^{(m)}$ can be dropped, resulting in a shortened intensity trace and therefore shorter image sequence from equation 11. But as the original image sequence can be permuted $2^{(m-1)}$ times before duplication of the output occurs, each filter level will still output 2N frames in total.

The appropriate number of filter levels to apply will depend on the chromophore blinking properties. Essentially one is trying to choose a time scale that covers the majority of emitter 'On' times. The procedure can therefore be continued for the 3rd, 4th or higher levels (corresponding to 4, 8 16... frame comparisons) but past the 5th level the number of emitters that are 'On' long enough becomes small unless the chromophore has poor blinking properties or the buffer conditions are far from optimal. However there is little disadvantage to choosing more filter levels other than the increase in image sequence size and associated analysis time. In practice where the original total number of frames N may be 10^4 or more calculation of the HWT can be computationally intensive. The image sequence is can therefore divided into smaller sections (eg 256 frames). Each section is processed separately and the results appended to a single image sequence. This also prevents discarding too many frames if N is not a power of 2.

Once the desired number of filter levels has been applied, the output image sequence can be analysed in the normal way using any single or multi emitter fitting algorithm, or a nonlinear image processing technique such as SOFI or SRRF. The only difference when performing fitting is that since the background has been removed the camera base level should be set to zero. Additionally filtering, particularly the first (m=1) filter level, increases the relative contribution of noise (shot, readout etc.) to the pixel intensity traces. This may produce relatively high intensity single pixels in the processed images, particularly if the emitter brightness in the original sequence is low. A localisation algorithm may try to fit these (as very narrow) or diffuse clusters of these (as very broad) as emitter PSFs. If the algorithm supports it, improvements in reconstruction image quality can be obtained by omitting localisations with non-physically broad or narrow PSFs to a greater degree than with unprocessed data, whilst still leaving a greater number of localisations than in unprocessed data. As the false-noise induced localisations are generally of lower intensity than 'real' emitter signals (unless the signal to noise is very low). Filtering out low intensity localisations is also effective (to a lesser degree) and is compatible with the astigmatic lens method of 3D localisation microscopy.